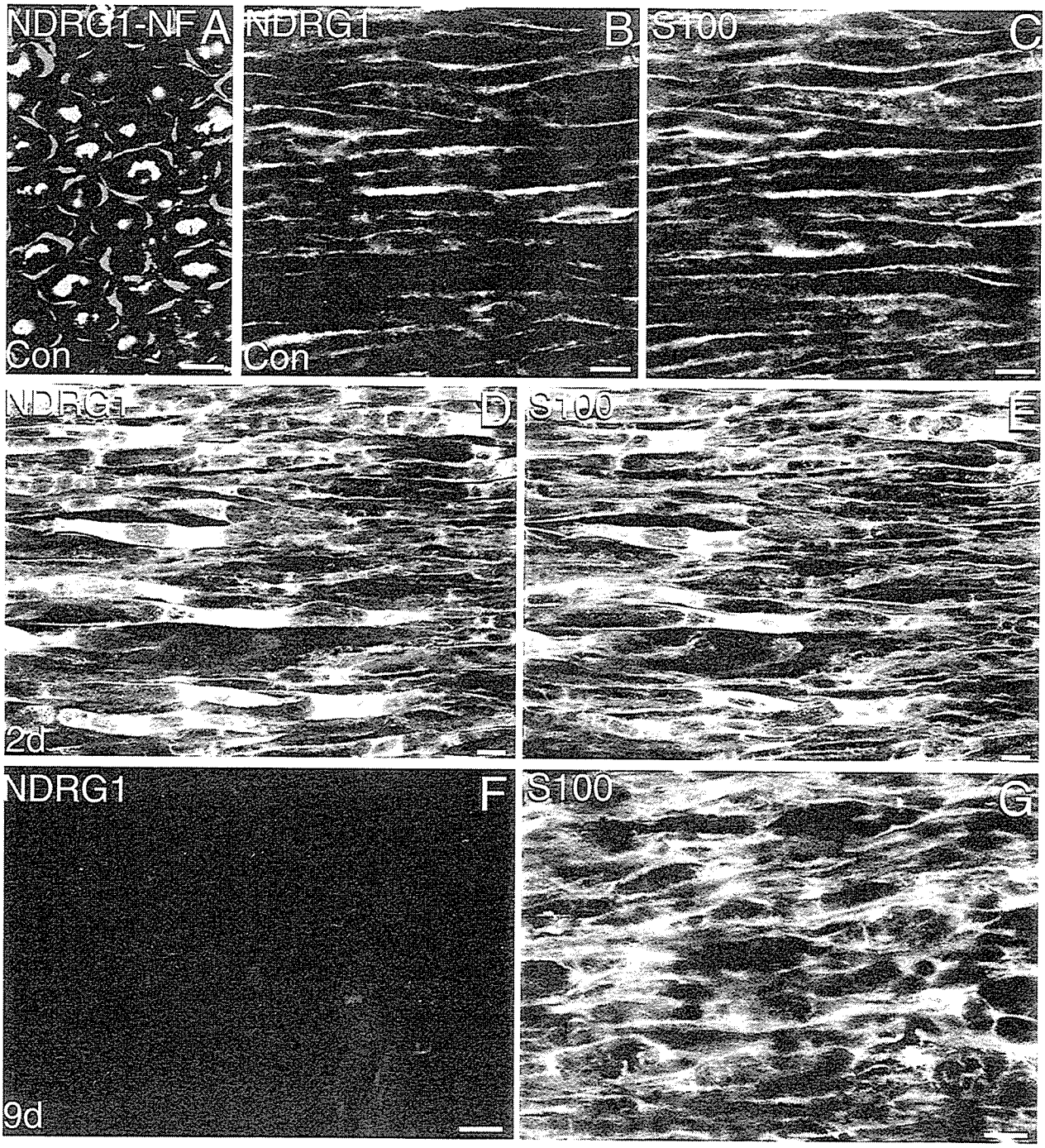

Fig. 3. Gray scale image of double immunofluorescent labeling of NDRG1 and NF in a transverse section of an intact nerve (A) and grayscale images of NDRG1 (B,D,F) and S-100 (C,E,G), in which each of the images is separately displayed, in longitudinal sections of an intact nerve (B,C) and the distal stumps of nerves at 2 days (D,E) and 9 days (F,G) after crush injury. **A–C:** In intact nerves the distribution of NDRG1 (gray in A) and NF immunoreactivity (white in A) is clearly distinguished, since the former is seen in the periphery (cf. Fig. 2A') of the round profile of each fiber and the latter is in the center. On the other hand, the NDRG1-ir sites (B) are almost identical to the S-100-ir sites (C), suggesting that NDRG1 is localized in the cytoplasm of Schwann cells, but not in axons. **D–G:** At 2 days, the expression of NDRG1 (D) is maintained in the S-100-ir Schwann cells which have transformed into myelin-phagocytosing cells (E), but at 9 days, the expression (F) is hardly detected in S-100-ir Schwann cells with a irregular profile (G). Scale bar = 10 μm.

carcinoma BeWo (Xu et al., 1999). The expression of NDRG1 protein was upregulated in the macrophage differentiation of leukemic U937 cells induced by treatment with 1,25-$(OH)_2$ vitamin D_3 or retinoic acid (Piquemal et al., 1999). Furthermore, stable transfection of a colon cancer cell line with NDRG1 cDNA

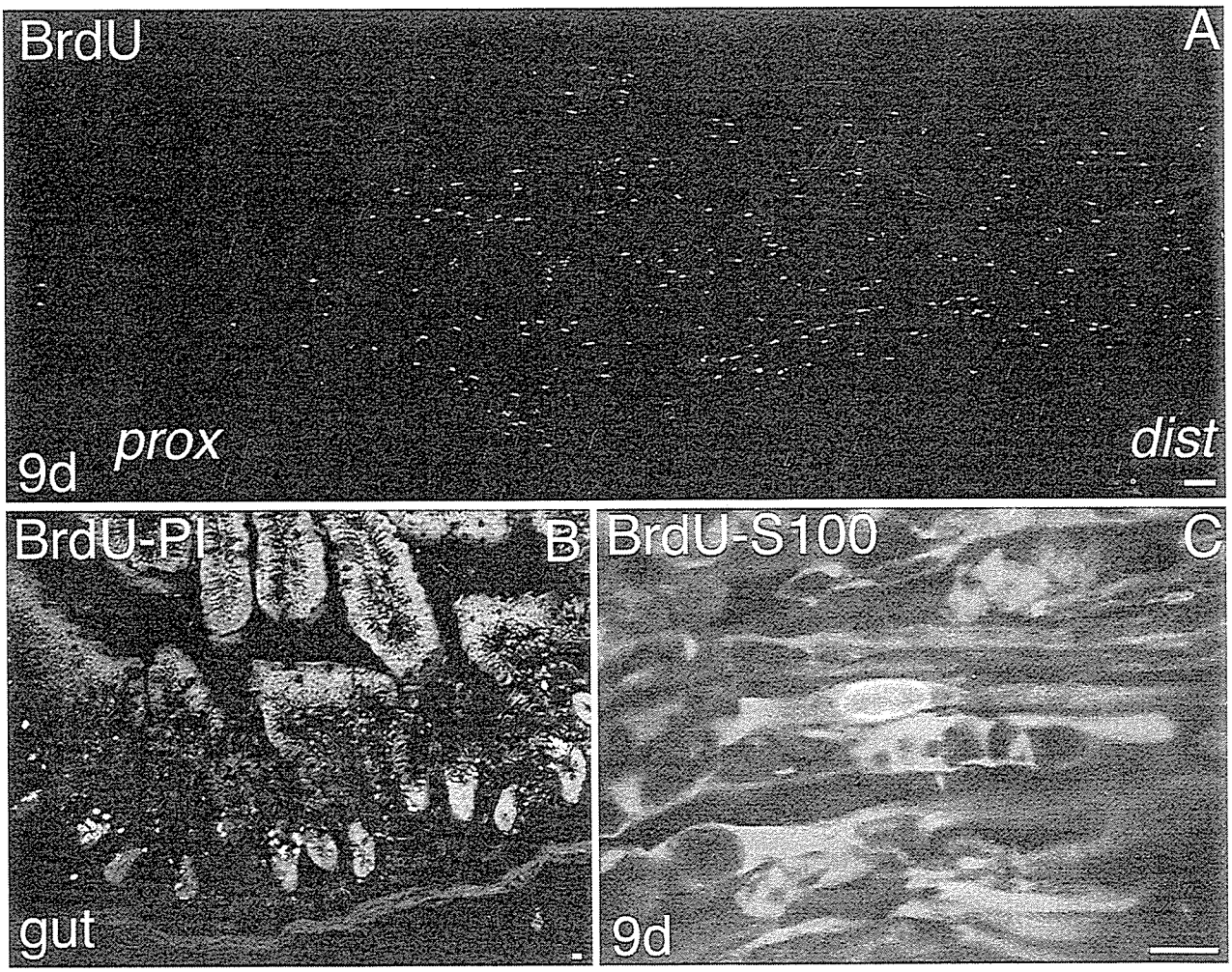

Fig. 4. BrdU immunofluorescent labeling of the nerve at 9 days after crush injury (**A,C**) and normal mouse jejunum as a positive control (**B**). **A:** In a longitudinal section of the nerve BrdU-labeled cells (white) are only distributed in the distal stump and the injury site, corresponding to the area where a marked depletion of NDRG1 is seen (cf. Fig. 1C). **B:** In a transverse section of the gut BrdU-labeled epithelial cells (white) are only located in the base of the crypts, to which cell proliferation is known to be restricted. Gray indicates PI-stained structures. **C:** In a higher-magnification image of the distal stump the double immunofluorescent labeling of BrdU (white) and S-100 (gray) shows that the nucleus of an S-100-ir cell is positive for BrdU, suggesting the mitotic activity of Schwann cells. Scale bars = 50 μm in A; 10 μm in B,C.

induced morphological and phenotypic changes indicative of differentiation, suggesting its possible role as a metastatic suppresser gene (Guan et al., 2000). Kurdistani et al. (1998) demonstrated that this gene was a p53-responsive gene with anti-proliferative properties, and that it was regulated in a cell cycle-dependent manner. These in vitro findings were supported by in vivo observations using in situ hybridization or immunohistochemical techniques showing that NDRG1 was expressed in the terminally differentiated cells in some organs, in which cell renewal is detectable under physiological conditions, such as colon epithelial cells (van Belzen et al., 1997), and skin keratinocytes (Gomez-Casero et al., 2001). Our immunohistochemical study on injured sciatic nerves revealed that the expression of NDRG1 was depleted in de-differentiated SCs and recovered in re-differentiated SCs with more immunoreactivity than that in the SCs of intact nerves. Thus, our findings suggest a role for NDRG1 in the terminal differentiation, including myelination, of SCs in nerve regeneration.

In a patient with HMSNL in whom a premature termination codon of the NDRG1 gene was found, one of the main neuropathological features of the disease was SC dysfunction, such as hypomyelination and demyelination/remyelination, failure of compaction of the innermost myelin lamellae, and poor hypertrophic response to the demyelination process (Kalaydjieva et al., 2000). It seems reasonable to surmise that this may be a direct effect of NDRG1 dysfunction, because this protein resides in SCs, especially myelinating ones. Kalaydjieva et al. (2000) inferred that the putative phosphopantetheine-binding domain present in NDRG1 protein (Kokame et al., 1996) may possibly be involved

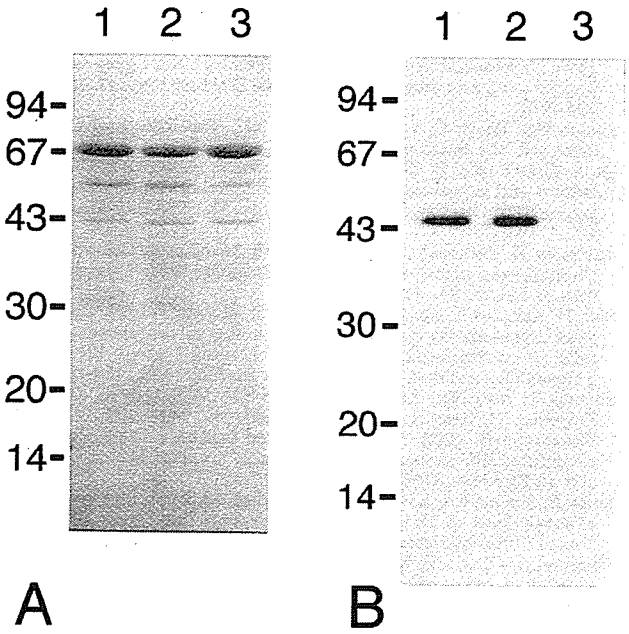

Fig. 5. Immunoblotting analysis of mouse sciatic nerves with a rabbit pAb to NDRG1. The samples were obtained at 9 days after crush injury. The amido black-stained sodium dodecyl sulfate-polyacrylamide gel electrophoresis (SDS-PAGE) profiles (**A**) and immunoblotted samples (**B**) from the intact side (**lane 1**), and the proximal stump (**lane 2**) and distal stump (**lane 3**) of the operated side are shown. The molecular weight markers (kDa) are indicated on the left.

in the lipid biosynthetic pathways operating in the myelinating SCs. On the other hand, Lachat et al. (2002) pointed out that the decompaction of the myelin sheath in the disease may be due to dysfunction of the adherens junctions in Schmidt-Lanterman incisures (Colman et al., 2001) based on their immunohistochemical findings that in all the examined epithelial cell types membrane labeling was observed predominantly adjacent to adherens junctions. Another prominent neuropathological feature of HMSNL is axonal involvement, such as early, severe, and progressive axonal loss (Kalaydjieva et al., 2000). Kalaydjieva et al. (2000) interpreted that NDRG1 may also have a role in the PNS, possibly in the SC signaling necessary for axonal survival, from their assumption that NDRG1 is possibly involved in SC differentiation, since differentiating SCs are an important source of signals for the development of nerves, in addition to controlling neuronal survival (Jessen and Mirsky, 1999). Our findings for NDRG1 expression in the process of nerve regeneration appear to support their hypothesis. However, further study is needed to clarify the exact role of NDRG1 in nerve development, since recent studies have stressed that the developmental process of the nerves is not always identical to the regenerative process, especially regarding the molecular mechanisms regulating SC proliferation (Kim et al., 2000; Atanasoski et al., 2001).

Besides the involvement of the NDRG1 in cell differentiation, this gene has been reported to be modulated under conditions of cellular stress that were caused by homocysteine (Kokame et al., 1996; Agarwala et al., 2000), forskolin (Xu et al., 1999), androgen (Segawa et al., 2002), nickel exposure (Salnikow et al., 2000), and hypoxia (Salnikow et al., 2000; Lachat et al., 2002). Our previous studies demonstrated that two different kinds of heat shock proteins (HSPs), 32 kDa-heat shock protein (Hirata et al., 2000) and 27 kDa-heat shock protein (Hirata et al., 2003) were differentially induced in different phases of SCs after axotomy, since the former was induced in SCs that transformed into myelin-phagocytosing cells immediately after the injury, while the latter was induced in SCs in the next phase that formed the SC column for axonal guidance. In the present study, NDRG1 was reexpressed during remyelination with more immunoreactivity than the normal level, suggesting its involvement in myelination, which is the last phase of SC transformation. No previous investigators have reported that the NDRG1 belongs to the HSPs. However, it is likely that, in addition to HSP32 and HSP27, this protein could be acting as a molecular base, explaining the inherent ability of SCs to not only protect themselves from abnormal environments but also participate actively in the repair process, although it may play a role in maintaining tissue homeostasis in intact nerves.

ACKNOWLEDGMENTS

The authors thank Mr. Yasuhiro Hirakawa and Mr. Takaaki Kanemaru (Morphology Core, Graduate School of Medical Sciences, Kyushu University) for their help in preparing the photomicrographs, and Mr. Naoya Inakura for his expert technical assistance.

REFERENCES

Agarwala KL, Kokame K, Kato H, Miyata T. 2000. Phosphorylation of RTP, an ER stress-responsive cytoplasmic protein. Biochem Biophys Res Commun 272:641–647.

Atanasoski S, Shumas S, Dickson C, Scherer SS, Suter U. 2001. Differential cyclin D1 requirements of proliferating Schwann cells during development and after injury. Mol Cell Neurosci 18:581–592.

Bandyopadhyay S, Pai SK, Gross SC, Hirota S, Hosobe S, Miura K, Saito K. Commes T, Hayashi S, Watabe M, Watabe K. 2003. The Drg-1 gene suppresses tumor metastasis in prostate cancer. Cancer Res 63:1731–1736.

Colman DR, Pedraza L, Yoshida M. 2001. Concepts in myelin sheath evolution. In: Jessen KR, Richerdson WD, editors. Glial cell development. 2nd ed. Oxford: Oxford University Press. p 161–176.

Fawcett JW, Keynes RJ. 1990. Peripheral nerve regeneration. Annu Rev Neurosci 13:43–60.

Gomez-Casero E, Navarro M, Rodriguez-Puebla ML, Larcher F, Paramio JM, Conti CJ, Jorcano JL. 2001. Regulation of the differentiation-related gene Drg-1 during mouse skin carcinogenesis. Mol Carcinogen 32:100–109.

Guan RJ, Ford HL, Fu Y, Li Y, Shaw LM. Pardee AB. 2000. Drg-1 as a differentiation-related, putative metastatic suppressor gene in human colon cancer. Cancer Res 60:749–755.

Hirata K, Kawabuchi M, 2002. Myelin phagocytosis by macrophages and nonmacrophages during Wallerian degeneration. Microsc Res Tech 57:541–547.

Hirata K, Mitoma H, Ueno N, He J, Kawabuchi M. 1999. Differential response of macrophage subpopulations to myelin degradation in the injured rat sciatic nerve. J Neurocytol 28:685–695.

Hirata K, He J, Kuraoka A, Omata Y, Hirata M, Shariful Islam ATM, Noguchi M, Kawabuchi M. 2000. Heme oxygenase 1 (HSP-32) is induced in myelin-phagocytosing Schwann cells of injured sciatic nerves in the rat. Eur J Neurosci 12:4147–4152.

Hirata K, He J, Hirakawa Y, Liu W, Wang S, Kawabuchi M. 2003. HSP27 is markedly induced in Schwann cell columns and the associated regenerating axons. Glia 42:1–11.

Jessen KR, Mirsky R. 1999. Schwann cells and their precursors emerge as major regulators of nerve development. Trends Neurosci 22:402–410.

Kalaydjieva L, Gresham D, Gooding R, Heather L, Baas F, de Jonge R, Blechschmidt K, Angelicheva D, Chandler D, Worsley P, Rosenthal A, King RH, Thomas PK. 2000. N-myc downstream-regulated gene 1 is mutated in hereditary motor and sensory neuropathy-Lom. Am J Hum Genet 67:47–58.

Kim HA, Pomeroy SL, Whoriskey W, Pawlitzky I, Benowitz LI, Sicinski P, Stiles CD, Roberts TM. 2000. A developmentally regulated switch directs regenerative growth of Schwann cells through cyclin D1. Neuron 26:405–416.

Kokame K, Kato H, Miyata T. 1996. Homocysteine-respondent genes in vascular endothelial cells identified by differential display analysis. GRP78/BiP and novel genes. J Biol Chem 271:29659–29665.

Krauter-Canham R, Bronner R, Evrard JL, Hahne G, Friedt W, Steinmetz A. 1997. A transmitting tissue- and pollen-expressed protein from sunflower with sequence similarity to the human RTP protein. Plant Sci 129:191–202.

Kurdistani SK, Arizti P, Reimer CL, Sugrue MM, Aaronson SA, Lee SW. 1998. Inhibition of tumor cell growth by RTP/rit42 and its responsiveness to p53 and DNA damage. Cancer Res 58:4439–4444.

Lachat P, Shaw P, Gebhard S, van Belzen N, Chaubert P, Bosman FT. 2002. Expression of NDRG1, a differentiation-related gene, in human tissues. Histochem Cell Biol 118:399–408.

Lin TM, Chang C. 1997. Cloning and characterization of TDD5, an androgen target gene that is differentially repressed by testosterone and dihydrotestosterone. Proc Natl Acad Sci USA 94:4988–4993.

Melhem MF, Meisler AI, Finley GG, Bryce WH, Jones MO, Tribby II, Pipas JM, Koski RA. 1992. Distribution of cells expressing myc proteins in human colorectal epithelium, polyps, and malignant tumors. Cancer Res 52:5853–64.

Nishie A, Masuda K, Otsubo M, Migita T, Tsuneyoshi M, Kohno K, Shuin T, Naito S, Ono M, Kuwano M. 2001. High expression of the Cap43 gene in infiltrating macrophages of human renal cell carcinomas. Clin Cancer Res 7:2145–2151.

O'Daly JA, Imaeda T. 1967. Electron microscopic study of Wallerian degeneration in cutaneous nerve caused by mechanical injury. Lab Invest 17:744–766.

Okuda T, Kondoh H. 1999. Identification of new genes ndr2 and ndr3 which are related to Ndr1/RTP/Drg1 but show distinct tissue specificity and response to N-myc. Biochem Biophys Res Commun 266: 208–215.

Piquemal D, Joulia D, Balaguer P, Basset A, Marti J, Commes T. 1999. Differential expression of the RTP/Drg1/Ndr1 gene product in proliferating and growth arrested cells. Biochim Biophys Acta 1450: 364–373.

Potten CS, Booth C, Pritchard DM. 1997. The intestinal epithelial stem cell: the mucosal governor. Int J Exp Pathol 78:219–243.

Qu X, Zhai Y, Wei H, Zhang C, Xing G, Yu Y, He F. 2002. Characterization and expression of three novel differentiation-related genes belong to the human NDRG gene family. Mol Cell Biochem 229:35–44.

Salnikow K, Blagosklonny MV, Ryan H, Johnson R, Costa M. 2000. Carcinogenic nickel induces genes involved with hypoxic stress. Cancer Res 60:38–41.

Sato N, Kokame K, Shimokado K, Kato H, Miyata T. 1998. Changes of gene expression by lysophosphatidylcholine in vascular endothelial cells: 12 up-regulated distinct genes including 5 cell growth-related, 3 thrombosis-related, and 4 others. J Biochem 123:1119–26.

Segawa T, Nau ME, Xu LL, Chilukuri RN, Makarem M, Zhang W, Petrovics G, Sesterhenn IA , McLeod DG, Moul JW, Vahey M, Srivastava S. 2002. Androgen-induced expression of endoplasmic reticulum (ER) stress response genes in prostate cancer cells. Oncogene 21:8749–8758.

Shaw E, McCue LA, Lawrence CE, Dordick JS. 2002. Identification of a novel class in the alpha/beta hydrolase fold superfamily: the N-myc differentiation-related proteins. Proteins 47:163–168.

Shimono A, Okuda T, Kondoh H. 1999. N-myc-dependent repression of ndr1, a gene identified by direct subtraction of whole mouse embryo cDNAs between wild type and N-myc mutant. Mech Dev 83:39–52.

Stoll G, Griffin JW, Li CY, Trapp BD. 1989. Wallerian degeneration in the peripheral nervous system: participation of both Schwann cells and macrophages in myelin degradation. J Neurocytol 18:671–683.

Ulrix W, Swinnen JV, Heyns W, Verhoeven G. 1999. The differentiation-related gene 1, Drg1, is markedly upregulated by androgens in LNCaP prostatic adenocarcinoma cells. FEBS Lett 455:23–26.

van Belzen N, Dinjens WN, Diesveld MP, Groen NA, van der Made AC, Nozawa Y, Vlietstra R, Trapman J, Bosman FT. 1997. A novel gene which is up-regulated during colon epithelial cell differentiation and down-regulated in colorectal neoplasms. Lab Invest 77:85–92.

Xu B, Lin L, Rote NS. 1999. Identification of a stress-induced protein during human trophoblast differentiation by differential display analysis. Biol Reprod 61:681–686.

Yamanaka I, Kuraoka A, Inai T, Ishibashi T, Shibata Y. 1997. Changes in the phosphorylation states of connexin43 in myoepithelial cells of lactating rat mammary glands. Eur J Cell Biol 72:166–173

Zhou D, Salnikow K, Costa M. 1998. Cap43, a novel gene specifically induced by Ni2+ compounds. Cancer Res 58:2182–2189.

Journal of the Peripheral Nervous System 9:144–157 (2004)

RESEARCH REPORT

The spatiotemporal characterization of endplate reoccupation, with special reference to the superposition patterns of the presynaptic elements and the postsynaptic receptor regions during muscle reinnervation

Songyan Wang, Masaru Kawabuchi, Chong Jian Zhou, Kazuho Hirata, Huibing Tan, and Akio Kuraoka

Department of Anatomy and Cell Biology, Graduate School of Medical Sciences, Kyushu University, Fukuoka, Japan

Abstract In this study, an immunohistochemical investigation was carried out to define spatiotemporal characteristics of superposition patterns of the presynaptic elements and the postsynaptic acetylcholine receptor (AChR) sites during the period of endplate regeneration after sciatic nerve crush. The extent of close correspondence of terminal Schwann cell (TSC)-, or axon terminal-, apposing AChR sites was quantitated with three-dimensional images of neuromuscular junctions (NMJs) taken under confocal laser-scanning microscopy. After 3-weeks post-crush (wpc), reoccupation of regenerating TSCs and later arriving axon terminals proceeded within the scope of previously denervated AChR plaques. During this period, the areas of presynaptic elements and the areas of postsynaptic elements were highly correlated. TSCs rapidly reoccupied a greater part of the postsynaptic receptors. In contrast, there was a slower increase of the contact areas of AChR sites overlapped by the axon terminals. Reoccupation by the presynaptic elements at 20 wpc was almost completed in a majority of NMJs, but some anomalous changes still continued to occur in a small proportion of the NMJs (20–30%). Our results suggest that: (a) with gradual increase of the contact areas between presynaptic and postsynaptic elements, imperfect reinnervation and regeneration, due to spatial mismatching or unbalanced growth between presynaptic and postsynaptic elements, result in sporadic remodeling; (b) the difference in superposition patterns between TSCs and axon terminals depends on the ability of making alignment to the endplate gutters in regenerating NMJs; and (c) a complex set of anatomical relationships among the three endplate components affects the process of endplate reoccupation synthetically.

Key words: acetylcholine receptor, immunohistochemistry, nerve regeneration, neuromuscular junction, Schwann cell

Introduction

In our recent study, the reinnervation of individual muscle fibers was investigated at various time points after the sciatic nerve was crushed *(Kawabuchi et al., 1998; 2001)*. After 3-weeks post-crush (wpc), the reinnervating Schwann cells (SCs) reoccupied damaged endplates by growing through the original SC tubes. At the later time, returned axons began to reoccupy damaged endplates, and over the following weeks, most endplates become gradually recovered. Terminal differentiation and endplate reoccupation were in process during the first few months of the reinnervation

Address correspondence to: Masaru Kawabuchi, MD, PhD, Department of Anatomy and Cell Biology, Graduate School of Medical Sciences, Kyushu University, Higashi Ku, Maidashi 3-1-1, Fukuoka 812-8582, Japan. Tel: +81-92-642-6045; Fax: +81-92-642-6050; E-mail: kawabuchi@helen.ocn.ne.jp

period, with a concomitant regenerative growth of the terminal SCs (TSCs) and the sites of clustered acetylcholine receptors (AChRs) *(Kawabuchi et al., 2001)*.

Normally, there is a precise spatial alignment between the presynaptic and postsynaptic elements in the vertebrate neuromuscular junctions (NMJs), which alters during remodeling, development, and regeneration. From the *in vivo* visualization study of the mammalian NMJs in living animals, the location of axon terminals, TSCs, and the distribution of AChR in the postsynaptic muscle fiber membrane were investigated during the period of muscle reinnervation *(Rich and Lichtman, 1989; O'Malley et al., 1999)* or muscle fiber growth *(Balice-Gordon and Lichtman, 1993)*. In both regeneration and growth, loss of AChR from a portion of the synapse precedes a rapid, partial loss of nerve terminal branches. In regeneration, the axon terminal precisely reoccupies the receptor regions in the old endplate site of the adult muscle *(Rich and Lichtman, 1989)*.

The three cellular components of NMJs, TSCs, motor axon terminals, and postsynaptic muscle fibers, are known to perform interaction that affects synapse formation, maintenance, and repair *(Hall and Sanes, 1993; Burden, 1998)*. The synaptic basal lamina contains a number of signaling proteins that influence motor nerve terminal differentiation during muscle reinnervation *(Sanes et al., 1978; Glicksman and Sanes, 1983; Sanes, 2003)*. The TSCs may regulate some aspects of differentiation and maintenance of axon terminals *(Jahromi et al., 1992; Rochon et al., 2001)* and synaptic plasticity *(Robbins and Polak, 1988)*. In addition, TSCs play a role in muscle reinnervation, and processes extended by TSCs after denervation influence the regrowth of motor axons to the muscles and their guidance back to denervated NMJs *(Son and Thompson, 1995a; 1995b; Trachtenberg and Thompson, 1997; O'Malley et al., 1999)*. At the same time, motor axon terminals also play a role in postsynaptic differentiation. Finally, it is generally agreed that besides providing the trophic support for neurons *(Grinnell and Herrera, 1981; Wernig and Herrera, 1986)*, feedback mechanisms from the muscle are important to anatomically or physiologically align neuromuscular synapses to their target cells *(Nudell and Grinnel, 1983; Slack et al., 1983; Hopkins et al., 1985; Crews and Wigston, 1990; Kuno, 1990)*.

Confocal three-dimensional (3D) images are useful for visualization and the morphological analysis of structures in regenerating NMJs. The advantage of this technique, compared with that performed by conventional fluorescence microscopy, is introduced below. Compared to normal junctions, regenerating neural elements are initially smaller and show various structural changes, such as uneven outlines and wide variability in size and terminal morphology. For those structures that originally have curvature and change with time, the 3D structure is more powerful in representing the true planar area of the endplate.

Knowledge of how TSCs or axons respond to nerve injury, particularly when reoccupation takes place on the once denervated postsynaptic receptor region, is important for understanding the formation and maintenance of regenerating NMJs. Following regeneration after nerve crush, the superimposed images of the TSC or axon terminal and AChR sites within the endplate of rat muscle were measured utilizing a dual-color confocal imaging technique *(Kawabuchi et al., 2001)*. In this study, we extend our previous observations by demonstrating some particular features of superposition of the presynaptic elements in relation to the postsynaptic elements in the spatiotemporal course of endplate reoccupation. In addition, the close correspondence (CC) between the pre- (TSC- or axon terminal-occupied region) and postsynaptic region was investigated quantitatively to define the difference in superposition patterns between the TSCs and axon terminals. Motor endplates were visualized by labeling the AChR sites with fluorescein isothiocyanate (FITC)-conjugated α-bungarotoxin (α-BT). Cryosections of the rat skeletal muscle were double-labeled with SC marker (S100) and α-BT, or with axonal marker (PGP9.5) and α-BT, and then observed using confocal laser-scanning microscopy. PGP9.5 is a suitable marker for detection of regenerating axons reinnervating in different target organs and is helpful for locating the major nerve pathways through target tissue (e.g., skin and muscle) *(Hirata et al., 1997; Navarro et al., 1997; Verdú and Navarro, 1997; Kawabuchi et al., 2001)*.

Despite return of motor nerve processes within weeks to months after peripheral nerve lesions, recovery of motor function is delayed for years *(Bowe et al., 1989)*. To evaluate the magnitude of restoration of the original motor function following peripheral nerve injury, long-term observations on the process of incomplete regeneration and reinnervation in NMJs need to be presented. In the present study, long-term alterations in the spatiotemporal course of endplate reoccupation, which persisted after regenerating axons grow into NMJs, were examined for up to 20 weeks.

Materials and Methods

Animals

All procedures were approved by the Committee of Ethics on Animal Experiments in the Faculty of Medicine, Kyushu University. Fifty adult male rats

(4 months old; body weight 315 ± 19 g, Wistar/Ms) were used for the experiments.

Surgery and tissue preparation

The procedures for nerve crush were the same as previously reported *(Kawabuchi et al., 1998)*. Under deep ether anesthesia followed by pentobarbital sodium (50 mg/kg body weight, subcutaneous injection), the right sciatic nerve was exposed and crushed for 20 s with microforceps. After nerve crush was achieved at the maximum pressure, the wound was sutured and animals were allowed to recover. At the time of perfusion, the operated leg muscles were found to become smaller than those of the control side in all cases in this study. A 15–25% reduction in muscle weights at 4 wpc was noted.

The animals were divided into several groups and allowed to survive for 1, 3, 4, 6, 8, 12, and 20 weeks post nerve crush. The soleus muscles from four to six rats were examined in each group; the muscles from control side served as control. In addition, 12 animals were divided equally into four groups, which were allowed to survive without operation for 4, 8, 12, and 20 weeks, to serve as negative controls. Three adult rats were used as sham operated ($n=3$) controls, where the nerve was exposed but not damaged. Following ether anesthesia and pentobarbital sodium, the animals were perfused through the aorta with phosphate-buffered saline (PBS) (pH 7.6) followed by 300–500 mL of fixative composed of 4% paraformaldehyde in 0.1 M phosphate buffer at pH 7.4. The muscles were dissected out and were then immersed in graded sucrose solution (up to 20% in 0.1 M phosphate buffer) for cryo-protection. A series of 50-μm-thick longitudinal serial sections were cut on a cryostat microtome (Frigocut, Germany) at −20 °C and were collected in PBS.

Immunohistochemistry

Sections were rinsed twice in PBS and once in 0.4% Triton-X 100 in PBS for 10 min, respectively, and then incubated in 1% bovine serum albumin (BSA) in PBS supplemented with 0.05% NaN_3 for 1 h. The following primary antibodies were applied to the sections for 24–48 h at room temperature: polyclonal anti-PGP9.5 (Ultraclone) diluted at 1 : 1,600–2,000 and polyclonal anti-S100 (Nichirei) diluted at 1 : 40. For detection of bound antibodies, the following procedures were used: sections were incubated with biotinylated secondary antisera (goat anti-rabbit IgG) diluted at 1 : 200 (Vector Laboratories, Burlingame, CA, USA) for 3 h, followed by streptavidin labeled with Texas red diluted at 1 : 200 (Vector Laboratories) for 2 h. Between each step, sections were washed three times in PBS for 15–30 min. All procedures were performed at room temperature (about 20 °C). The sections were placed on a slide pretreated with 0.1% Poly-L-Lysine (Sigma). Following immunostaining, the area of the postsynaptic AChR site was defined by FITC-conjugated α-BT staining for 1 h at 37 °C (dilution 1 : 200, Molecular Probes, Eugene, OR). Then sections were washed several times in PBS for 30 min and mounted with Vectashield (Vector, USA).

Confocal laser-scanning microscopy

Counterstained materials were observed with a confocal laser-scanning microscopy system (CLSM-GB 200 Olympus, Japan) equipped with an argon/krypton ion laser, allowing simultaneous scanning of two fluorescent dyes. In order to avoid any nonspecific cross-talk, observations of staining for either FITC or Texas red were made as the following: the wave length of the excitation laser light was restricted to 488 nm (argon laser) for FITC or to 568 nm (krypton laser) for Texas red separately by switching the dichroic mirrors. For simultaneous observations of the materials double-stained by FITC and Texas red, the serial images were taken under 488 nm and 568 nm laser lights separately on the same scope. Optical sections at intervals of 0.5–1 μm were projected on a single plane extending in 10–40 μm thickness. The series of optical sections were reconstructed to show superimposed images of the TSC and AChR site or axon terminal and AChR site. Using a 40× or 60× water immersion objective lens, the 3D structure of the motor endplate can be shown by reconstructing the series of images. It was noted that the areas of endplates on the adult muscle in 3D image are significantly larger than that in 2D image.

Morphometric analysis

For quantitative analysis of each of the three-dimensionally reconstructed junctional components, several sections in 50 μm thickness with the necessary number of NMJs were selected from each animal. To combine the data from different animals, all the sections from three to six animals in each group were processed for morphometry. In addition, it was determined that at least 15 NMJs per section and five sections per animal were required for statistical reliability to ensure that inter-animal variability was not significant. Only the motor endplates cut at the tangential plane were selected and images in which the entire motor endplate was parallel to the long axis of the muscle fiber were rejected. The area of motor endplate was defined as where the preterminal SCs or axons terminate on the AChR sites outlined by α-BT staining. One motor endplate was often organized into two or more groups, each of which contained a collection of terminal SCs or nerve terminal branches. To

avoid errors in statistical reliability, the motor endplates with undefined borders, due to distant neighboring groups of TSCs or axon terminals, were not counted. The area of an axon terminal included the projection area of the axon terminal and its branches at the AChR site, and the point of origin was defined as the first branch point of the axon terminal.

The time course of changes in sizes of S100-like immunoreactive TSCs, PGP9.5-like immunoreactive axon terminals, and α-BT-stained AChR sites was documented in our previous study *(Kawabuchi et al., 2001)*. In the present study, individual sizes during regenerative growth at 4, 8, 12, and 20 wpc, estimated from the extent of the longitudinal-sectional areas, were combined in a scatter diagram, and the distribution of individual value pairs for the area of presynaptic elements (TSCs or axon terminals) and AChR sites is shown (Fig. 1). The anatomical relationship between these parameters was analyzed by single-variance linear regression analysis. Single Texas red-stained S100- or PGP9.5-like immunoreactivity was normally red, but it would become yellow when structures

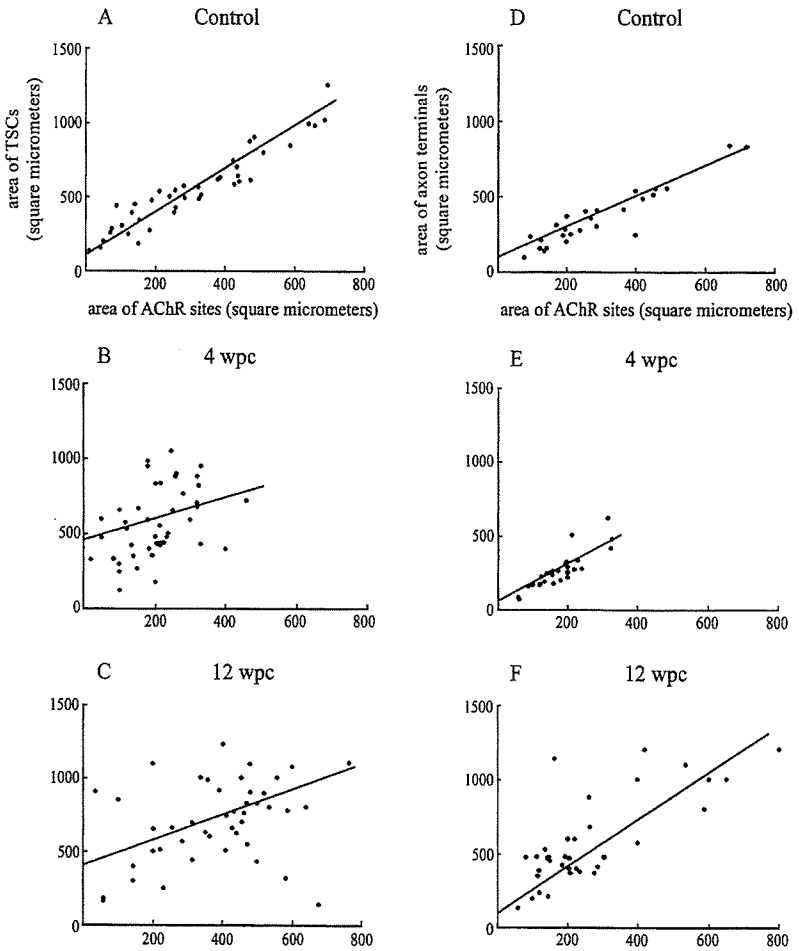

Figure1. Scatter diagrams of the relationship between area (μm^2) of acetylcholine receptor (AchR) sites (horizontal axis) and area of terminal Schwann cell (TSCs) (A–C) or area of axon terminals (D–F) in neuromuscular junctions (NMJs) (vertical axis). Measurements were performed on 90–150 samples from control (A and D), 4-weeks post-crush (wpc) (B and E) and 12 wpc (C and F) separately. The unit values are indicated by a square. The regression line is calculated from the pooled values of the two data sets. (A) The increase in area of the AChR sites in control correlates with that of the TSCs [r (correlation efficient) = 0.94, $p < 0.001$, two-tailed t-test, $n = 97$]. (B, C) The shift of individual value pairs at 4 and 12 wpc indicates that nerve crush induced a decrease in areas of AChR-rich sites and correlated changes in areas of TSCs ($r = 0.42$ at 4 wpc, $p < 0.001$, two-tailed t-test, $n = 62$; $r = 0.33$ at 12 wpc, $p < 0.01$, $n = 145$). The distribution of points at 12 wpc seems to be more dispersed than at 4 wpc. (D) A significant linear relationship is obtained between the two parameters in the control [r (correlation efficient) = 0.93, $p < 0.001$, two-tailed t-test, $n = 97$]. (E, F) At 4 and 12 wpc, there is the similar linear relationship between area of axon terminals and area of AChR sites in NMJs ($r = 0.86$ at 4 wpc, $p < 0.001$, two-tailed t-test, $n = 62$; $r = 0.75$ at 12 wpc, $p < 0.01$, $n = 145$). The shift of individual value pairs at 4 wpc indicates that nerve crush induced a coincidental decrease between TSCs and AChR plaques. (F) Note considerable correlated recovery in the 12-week muscles.

were identified by both Texas red staining and green FITC fluorescence, where superimposition of presynaptic elements and postsynaptic receptor regions existed. A schematic representation of the analysis for superimposed images from the region of CC, estimated by the programs Adobe Photoshop and NIH, is shown in Fig. 2. In order to make an easy morphometric analysis, the double-color images (see boxed regions in Fig. 3C,I) were converted to single-color image at first, by switching the multiple color channels to only one channel with Photoshop (green for FITC or red for Texas red). Then the single-color images were converted to gray (black and white) images by grayscale mode, which can show the areas of TSCs, axon terminals, or AChR sites separately (Fig. 2). In addition, for analysis of the superimposed yellow areas between TSC/AChR site or axon terminal/AChR site in double-color images (see boxed areas in Fig. 3), the double-color images were converted to gray images with Photoshop (Fig. 2). Then the gray images were processed by threshold mode, and the threshold intensity on the grayscale image was adjusted by density-slice filtering. With appropriate adjustment, the non-overlapped areas from presynaptic and postsynaptic elements were then taken away from the NMJ by digitally subtracting the binary image and the accurate superimposed areas were displayed (Fig. 2). Selected superimposed areas corresponding to the CC were

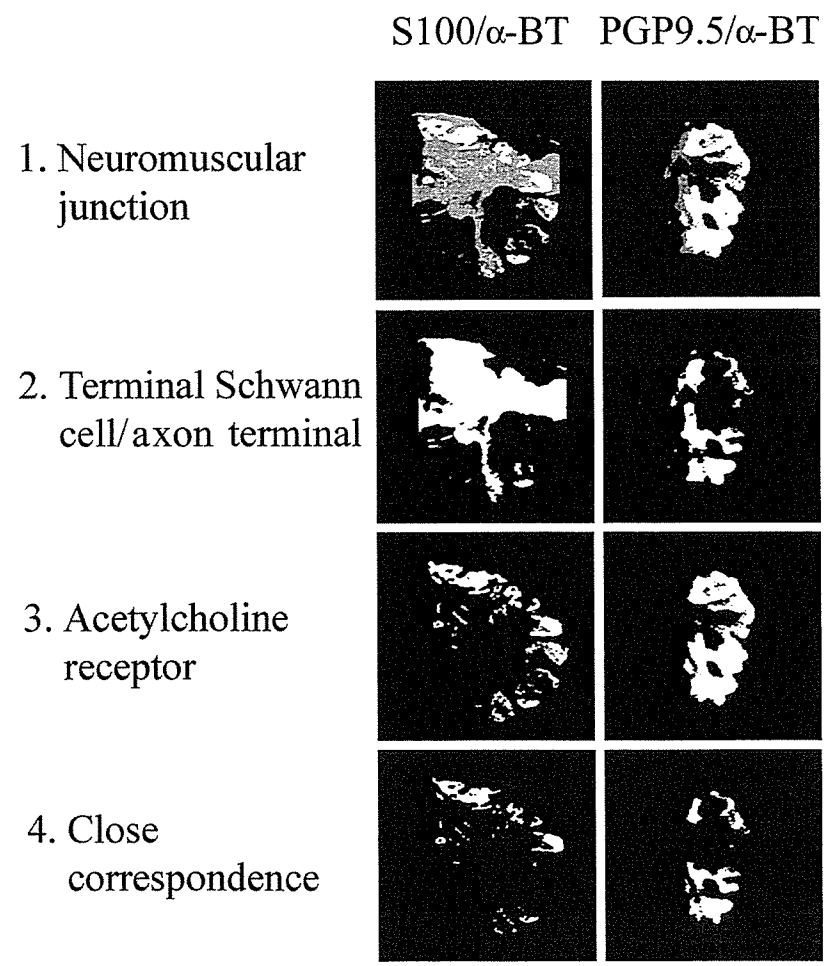

Figure 2. Diagrammatic procedure for estimating extent of close correspondence (CC) between pre- and postsynaptic elements of neuromuscular junctions (NMJs). The dual-color images of the original double-labeled fluorescent NMJs are from the boxed regions in Fig. 3(C,I). Terminal Schwann cells (TSCs) or axon terminals are shown in red, receptor regions in green, and the superimposed regions [CC with the postsynaptic acetylcholine receptor (AchR) sites] in yellow. (1) The original color images are converted to Gray images. (2), (3), and (4) grayscale images are converted to binary images, using an intensity threshold based on the mean background level. (2) The binary image of the TSC or axon terminal is digitally subtracted from the binary image of the NMJ. (3) The receptor regions demonstrate branches associated with disparate clusters of AChRs. (4) The area of CC is obtained by digitally subtracting the area of non-correspondence from the total area of the receptor region. In addition, the binary subtraction images in (4) are independently verified by referring to the original yellow-colored images in boxed areas of Fig. 3(C,I).

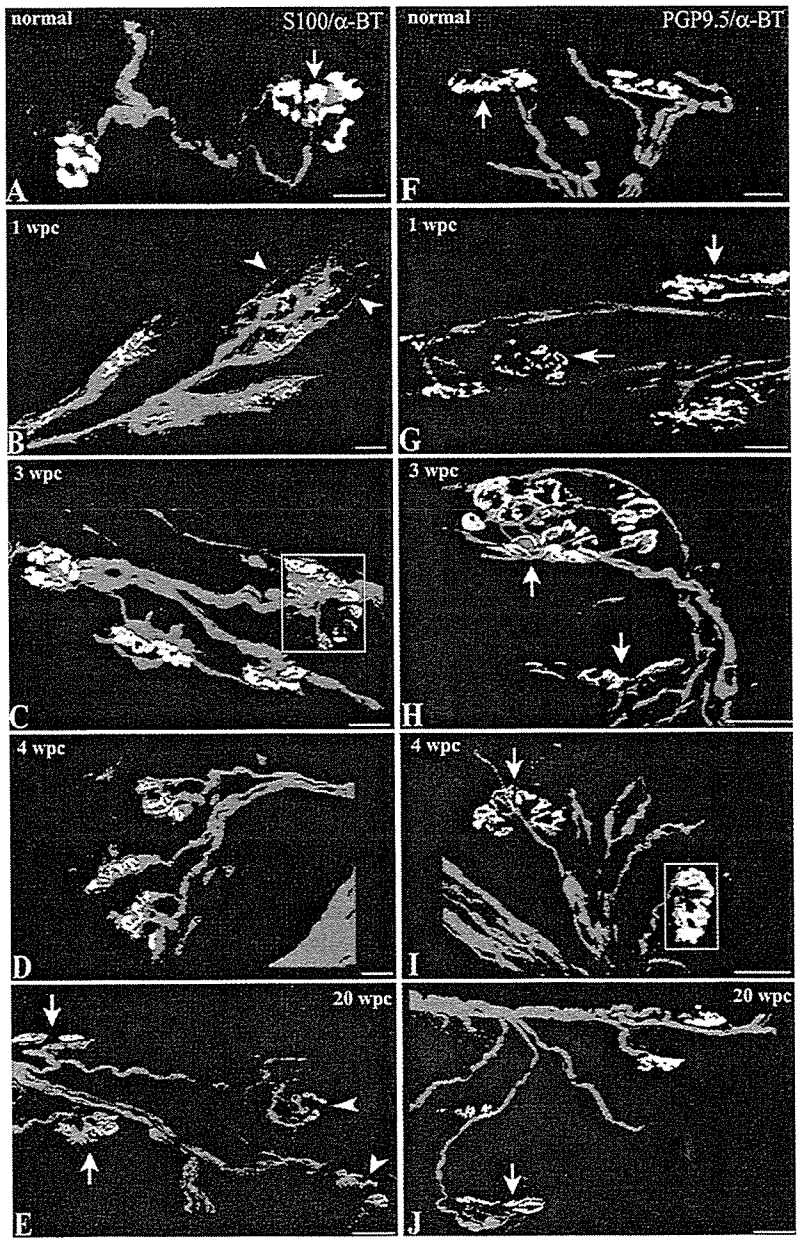

Figure 3. (A–E) Double-fluorescence labeling for S100 (red) and α-BT (green) in longitudinal sections of neuromuscular junctions (NMJs) at unoperated control (A), 1 (B), 3 (C), 4 (D), and 20 (E) weeks post-crush (wpc), and (F–J) double fluorescence labeling for PGP9.5 (red) and α-BT (green) at control (F), 1 (G), 3 (H), 4 (I), and 20 (J) wpc show the sequence of endplate reoccupation by S100-positive terminal Schwann cells (TSCs) and PGP9.5-positive axon terminals. The superimposed red and green images show superposition areas that appear yellow between SCs/axons and postsynaptic acetylcholine receptor (AchR) plaques. Note in all figures that TSCs or axon terminals invariably regenerate within the territory of AChR geometry. (A, F) NMJs (arrows) in unoperated controls. Note almost complete and accurate spatial occupation between nerve terminals [TSCs (A), axon terminals (F)] and postsynaptic receptor regions. (B) Loosely aligned TSCs with profuse robust extensions (arrowheads) overlie AChR sites with degeneration figures (shrinkage, fragmentation). (C–E) In most NMJs, TSCs are well organized and aligned with regular contours, indicating ongoing regeneration. (C, D) From early in reinnervation, the yellow-colored superposition predominates, indicating that the major area of the TSC profile closely contacts over the area of the AChR plaque. (E) At 20 wpc, some NMJs show almost complete superposition (arrows), while in others (arrowheads), less developed TSCs are coupled with poorly formed AChR plaques. (G) At 1 wpc, axon terminals are disorganized and disintegrated in a majority of NMJs, with AChR plaques being left unoccupied (arrows). (H–J) With advancement of endplate reoccupation, the terminal arborizations expand into a series of boutons and cover the entire NMJ area. (H, I) Early in reinnervation, superposition of the axon terminals and AChR sites (arrows) is seen. (J) At 20 wpc, despite advancement in superposition, poorly formed terminals, partially occupying an AChR plaque, still can be seen (arrow). The boxed regions in (C) and (I) were processed in Fig. 2. Scale bar = 20 μm.

measured. To minimize the subjective bias in delineation of the borders of the structure, the scope of the gray image was always referenced to that of the original color image (green, red, or yellow). Following measurement of the superimposed yellow area, the ratio of CC at 4, 8, 12, and 20 wpc was estimated by the quotient of the mean area of the yellow image divided by the green-colored AChR sites. Morphometric analyses of characters and relationship among three components of NMJ during muscle reinnervation were always referenced to the normal controls and were performed independently by two investigators on original images. Their results were compared to evaluate accuracy.

Statistics

The incidence of anomalous changes in TSCs and axon terminals, as expressed by a percent, were compared with the chi-square test at a level of significance of 99%. For the superposition areas delimited by TSCs or axon terminals, mean and standard deviations were calculated. Differences in the means of each parameter at 4, 8, and/or 12 wpc were compared with a two-tailed Student's *t*-test. Differences between the two values were considered significant if the probability value (p) was found to be less than 0.05.

Results

Correlation in size between presynaptic and postsynaptic elements

Nerve crush induced long-lasting atrophy of AChR sites in which their area, perimeter, and diameter significantly reduced from normal levels, and the degree of reduction in the area of the AChR site was prominent at 4 wpc, with subsequent restoration at 12 wpc *(Kawabuchi et al., 2001)*.

The distribution of individual value pairs of the areas of TSCs and AChR sites is shown by the scatter diagrams (Fig. 1A–C). A positive relation was most evident in controls, and sizes of AChR sites were significantly correlated with those of TSCs in controls [the correlation efficient (r) for endplate area and TSC size = 0.94, $p < 0.001$] (Fig. 1A). Across all the time points (4, 8, and 12 wpc), significant correlation was maintained during reinnervation following nerve crush ($r = 0.42$ at 4 wpc, $p < 0.001$; $r = 0.85$ at 8 wpc, $p < 0.001$; and $r = 0.33$ at 12 wpc, $p < 0.01$) (Fig. 1B,C). The area of most AChR sites decreased at 4 wpc and gradually recovered to the normal level. Compared with the decrease in the area of AChR sites, some areas of TSCs increased and the others decreased at 4 wpc. The relationship between both gradually became correlated as shown in the control.

At the same time, sizes of AChR sites were also significantly correlated with those of axon terminals (r for endplate area and axon terminal size = 0.93, $p < 0.001$) (Fig. 1D). The area of most axon terminals decreased with the decrease in AChR sites at 4 wpc. During muscle reinnervation, the increase in area of axon terminals obviously correlated with area of postsynaptic receptor region ($r = 0.86$ at 4 wpc, $p < 0.001$; $r = 0.54$ at 8 wpc, $p < 0.001$; and $r = 0.75$ at 12 wpc, $p < 0.001$) (Fig. 1E,F). The proportion of the small-sized axon terminals/AChR sites predominated at 12 wpc.

Anomalous superposition between TSCs (or axon terminals) and AChR sites in NMJs

During 4–20 wpc, we note that the magnitudes of endplate reoccupation between the pre- and postsynaptic sites greatly varied in NMJs, and some anomalous superposition figures emerged either accidentally or in groups within the muscle (Fig. 4A–I). For TSCs, we note that 1) regenerating TSCs overlapped either well-organized (Fig. 4C) or shrunken (Fig. 4F) AChR sites and 2) some of the AChR plaques showed signs of undifferentiation, such as flat, less intensely stained, and often wider than initially seen, without branching or segmentation to delineate the synaptic invaginations (Fig. 4I).

Uncoordinated spatial alignment in each of the disorderly regenerating axon terminals was a consistent feature (Fig. 5A–L), aside from those with complete reoccupation and close superposition (Fig. 5M–O). We note that major anomalous changes consisted of superposition of regenerating axon terminals with shrunken and less-developed AChR sites (Fig. 5A–F). In some NMJs, the branching area of the nerve terminal was great enough, but its greater part was not overlapped with the AChR site (Fig. 5A–C). At the same time, some AChR sites displayed were only partially occupied (Fig. 5D–F). (2) During this period, polyaxonally innervated NMJs were frequently found, including multiple extensions traveling through the same pathway into the same NMJ and sharing it. Each axon terminal sharing the same multiple innervated NMJ displayed similar but no identical pattern of superposition (Fig. 5J–L).

Statistics for incidence of anomalous superposition per junction

'Anomalous change' was defined as NMJs with greatly unoccupied AChR plaques with occupation ratios less than 50% and/or poorly formed endplate occupants. The time courses of number of anomalous changes per junction are shown in Fig. 6. The number of the TSC-related anomalous changes peaked at 4 and 6 wpc, with a subsequent later decline (Fig. 6A). In contrast, the incidence of anomalous axon

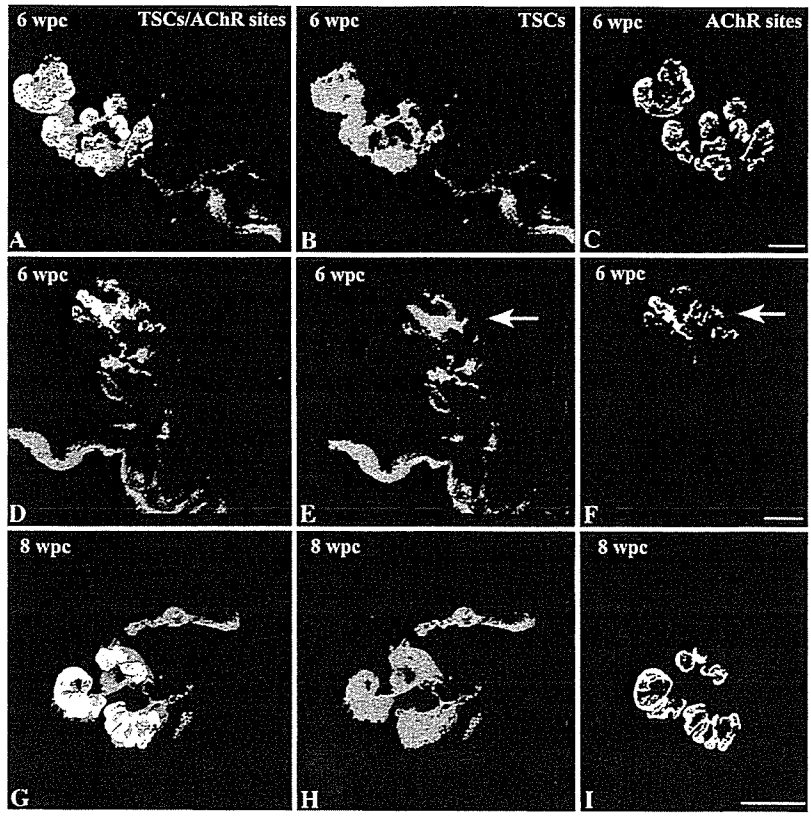

Figure 4. Anomalous figures during endplate realignment of terminal Schwann cell (TSC)/acetylcholine receptor (AchR) site at 6-weeks post-crush (wpc) (A–C, D–F) and 8 wpc (G–I). A, D, G: superimposed images. B, E, H: TSC profiles. C, F, I: AChR sites. (A–C) Ongoing endplate superposition is displayed between the TSC and AChR site. (D–F) Poorly developed TSCs are superimposed with poorly formed AChR sites, which manifest thin flat plaques and ill-defined contours (arrows). (G–I) TSCs with well-defined shapes and edges overlap an AChR plaque showing the lack of the usually segregated organizations, suggesting shallow branching and undeveloped synaptic infoldings. Scale bar = 20 μm.

terminal-related superposition displayed biphasic changes, peaking in the early (4 wpc) and late (12 and 20 wpc) reinnervation periods. The latter change was possibly derived from remodeling or adaptation of regenerating NMJs (Fig. 6B).

Delay in CC between axon terminals and AChR sites in NMJs during muscle reinnervation

In unoperated controls, the superimposition of nerve terminal staining over AChR sites showed that there was almost complete spatial occupation between nerve terminals and postsynaptic receptor regions, with very few pre- (the nerve terminal extending beyond the post-projection) or postsynaptic displacement (post-projection extending beyond the nerve terminal) (Fig. 3A,F).

Labeling for S100 in NMJs at 1 wpc clearly defined chain-like cellular strands as regenerating SC strands, and the junctional clusters of round or elliptical cells with profuse process extensions as TSCs (Fig. 3B). These TSCs overlapping AChR plaques mostly showed features of degeneration such as shrinkage and fragmentation. At 3 wpc, greater portions in regions of CC between the TSCs and AChR plaques displayed green-colored FITC fluorescence, indicating that S100 labeling only partially covered the area of AChR plaques at the NMJ (Fig. 3C). From 4 wpc, most NMJs became yellow-colored, where coverage of TSCs over the area of AChR plaques is almost complete (Fig. 3D–E). This endplate profile showed a consistent feature until 20 wpc, while fewer developed TSCs superimposed with fewer developed AChR plaques still persisted in some NMJs (Fig. 3E).

Comparison of the axon terminal-mediated superposition with that of TSCs indicated that the way in which the axon terminals branched to occupy the AChR sites was different. At 1 wpc, there was no or sparse labeling for PGP9.5 in NMJs, with only vacant AChR plaques being left (Fig. 3G). During 3–20 wpc, reoccupation of the axon terminals over the AChR plaques was in process. At 3 and 4 wpc, greater portions in regions of CC between the axon terminals

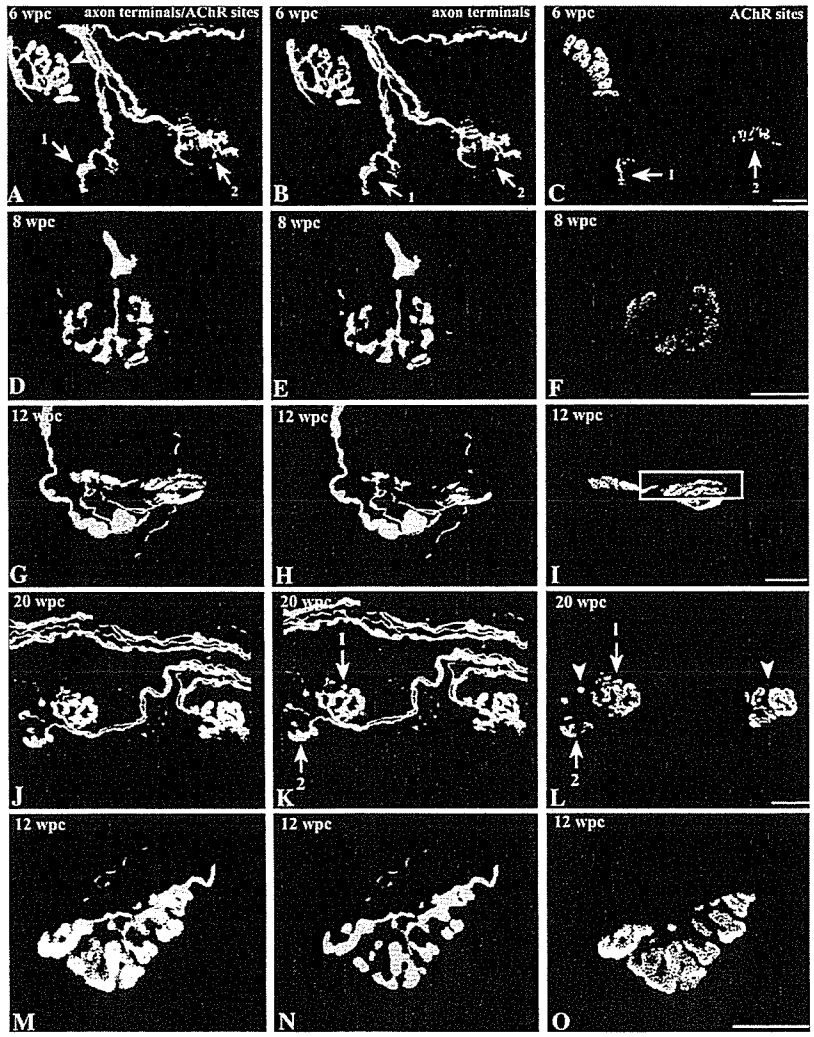

Figure 5. Anomalous changes during endplate realignment of axon terminal/acetylcholine receptor (AchR) site at 6- (A–C), 8- (D–F), 12-(G–I, M–O), and 20-weeks post-crush (wpc) (J–L). A, D, G, J, M: superimposed images. B, E, H, K, N: axon terminals. C, F, I, L, O: AChR sites. (A–C) Besides normally occupied neuromuscular junctions (NMJs) (arrowhead), there is a wide variability in degree of superposition at poorly developed NMJs. In the two junctions (arrows 1 and 2), well-developed terminal arbors greatly contrast with the poorly formed AChR plaques. (D–F) Regenerating terminal arbor overlaps an AChR plaque manifesting granular distribution with the frayed border. (G–I) The boxed region of an AChR plaque, displaying shrinkage and simplicity, remains unoccupied by the axon terminal, indicating discrepancy in sizes of individual endplate occupants. (J–L) Superposition patterns from polyaxonally innervated NMJs, where two or more extensions travel up the same course to the NMJ. Multiple innervated NMJs show well-regenerated terminals, while individual terminal plaques sharing the same NMJ (arrows 1 and 2) display similar though not identical superposition patterns. (L) The simplified structures (right arrowhead) and a few small round or spindle-shaped plaques (left arrowhead) in AChR sites are estimated as signs of reconstruction. (M–O) Fully regenerated anatomical relations in the later reinnervation period. Scale bar = 20 μm.

and AChR plaques mostly displayed green-colored FITC fluorescence, indicating that axon terminals only partially occupied the limited area of AChR plaques (Fig. 3H–I). Progressively, more area of the postsynaptic receptor region was covered by well-defined and elaborate arborizations of axon terminals, and endplate reoccupation was almost complete in 90% of the NMJs at 20 wpc (Fig. 3J).

Statistics for area of CC per junction

The rates of increase in the extent of superposition areas that follows reinnervation were not proportionate between TSCs and axon terminals (Fig. 7). The pattern of CC of the TSCs or axon terminals in unoperated controls was similar to that seen in the sham controls. At 4 wpc, the mean superposition areas of the TSCs compared with mean control values showed a 20% increase (158/131, $p < 0.001$, *t*-test); however, those

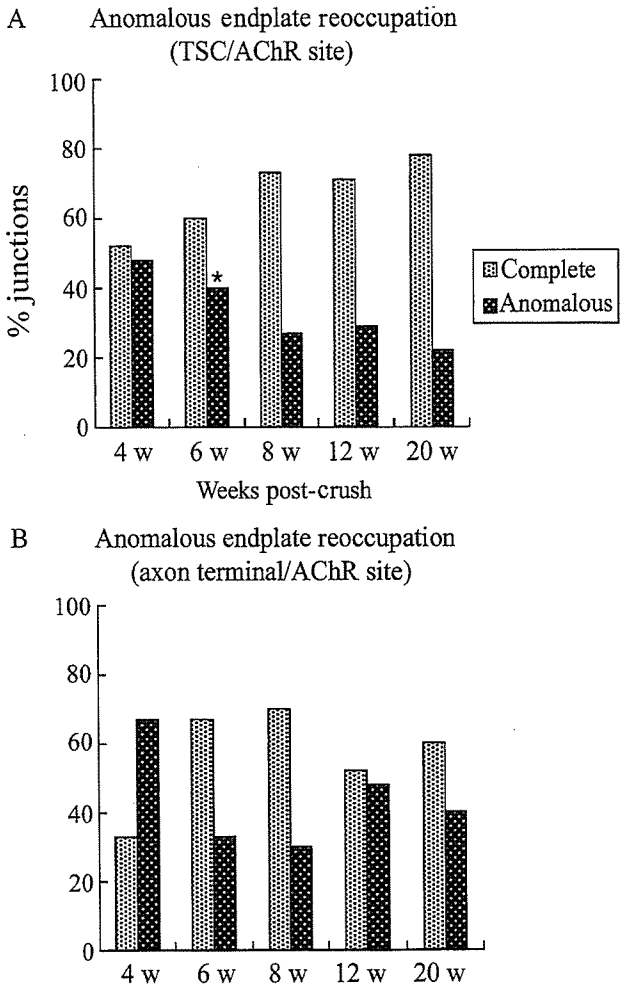

Figure 6. Bar graphs showing time courses of the incidence of anomalous changes during endplate reoccupation, such as greatly unoccupied endplates and/or less developed occupants. The incidence, in respect to the total number of neuromuscular junctions (55–90), was measured. (A) As for the number (mean percent) of anomalous changes per terminal Schwann cell-apposing junction, the peak at 4-weeks post-crush (wpc) and 6 wpc shows a subsequent decline (6 vs. 8, 12 or 20 weeks, *$p < 0.001$, chi-square test). (B) In the axon terminal-apposing junctions, the anomalous incidence shows the prominent rise in the early (4 wpc) and late reinnervation period (12 and 20 wpc).

of the axon terminals decreased by 45% (73/162, $p < 0.001$) (Fig. 7A,B). For TSCs, the increases with a subsequent decline to normal level during the period suggest that regenerating TSCs attained wider superposition areas than in controls, besides rapidly restoring contact areas to the postsynaptic receptor regions. But compared with TSCs, it was remarkable that the mean superposition areas of regenerating axon terminals were consistently smaller than controls, with gradual return to control levels [81% (125/154) at 8 weeks and 86% (155/180) at 20 weeks] (Fig. 7B).

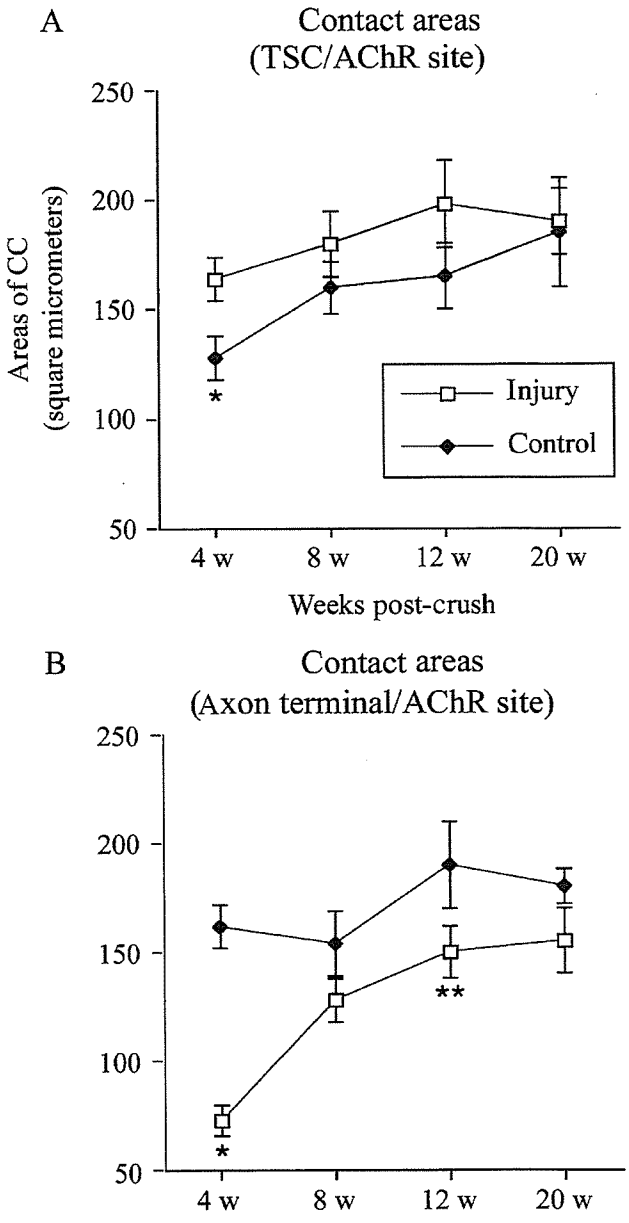

Figure 7. Extent of close correspondence (CC) delineated by terminal Schwann cells (TSCs) (A) or axon terminals (B) at 4-, 8-, 12-, and 20-weeks post-crush (wpc). Values (μm^2) are expressed by the mean area ± standard error of CC among the total number of junctions. A total of 60–75 junctions were evaluated per time point. (A) Compared with controls, contact areas of TSC/acetylcholine receptor sites show increases until 20 wpc, possibly due to growth and remodeling of junctions. Values at 4 wpc already are over normal levels (control vs. 4 wpc, *$p < 0.025$) and at 20 wpc recover to normal levels. (B) As compared with controls, areas of axon terminals show decline, especially at 4 (*$p < 0.025$) and 12 wpc (**$p < 0.05$).

Statistics for ratio of CC per receptor region

The time courses of the ratios of CC delimited by TSCs or axon terminals to the geometry of AChR

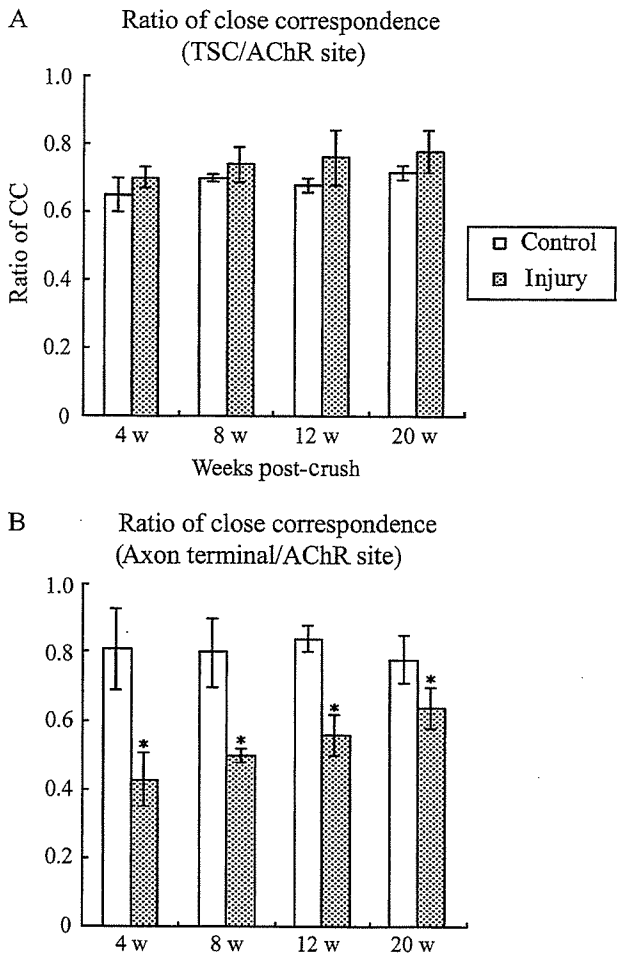

Figure 8. Available contact areas of neuromuscular junctions (NMJs) are estimated by the ratio of close correspondence (CC) at 4-, 8-, 12-, and 20-weeks post-crush (wpc). The ratio of CC is expressed by the quotient of the mean area (μm^2) of superposition from terminal Schwann cells (TSCs) or axon terminals divided by the mean area of acetylcholine receptor sites, respectively. (A, B) In controls, junctions are almost completely occupied and values of ratio of CC are stable around 0.7 (A) or 0.8 (B). (A) After injury, ratios of CC of TSC always appear a little greater than controls, though statistically insignificant. (B) In contrast to TSCs, ratios of CC of axon terminal at 4, 8 and 12 wpc are reduced. Despite gradual recovery, they are still less than normal levels at 20 wpc. *denotes statistically significant difference from the control values ($p < 0.001$).

plaques, estimated by the mean areas of superposition divided by mean areas of the AChR site, are shown in Fig. 8. After 4 wpc, values of TSCs both in control and injured models displayed constantly higher levels (>0.7), especially a persistent greater value of operated groups than controls (Fig. 8A), which was basically consistent with that seen in the rapid and smooth spatial realignment of regenerating NMJs as shown in Fig. 7. The ratios of CC of axon terminals showed a pronounced decline at 4 wpc (controls vs. axon terminals at 4 weeks, 0.82 vs. 0.42) with gradual return to control levels, indicating that the rate of reoccupation in axon terminals over the geometry of the AChR plaques was delayed.

Variability of data between the two independent researchers

In order to make the morphometric analyses of the area of CC and the incidences of anomalous endplate changes, the sections from each group at different time points were measured and analyzed by one investigator and then were examined independently once again by another investigator. There was no discernible difference in the measured data, and the minor discrepancy (3–7%) between these two independent observations was from the deviation in identification of the territory of the terminals, or the overlooking of faintly stained fine neural profiles arising from axon terminals or TSCs, which should be included as a positive count at last.

Discussion

Regenerative endplate growth coupled with remodeling

On the basis of the *in vivo* visualization study of reinnervating NMJs, Rich and Lichtman *(1989)* reported that the original endplate site was always the site of reinnervation and the reinnervating nerve occupied all of the original synaptic sites. Our recent study showed that the endplate regeneration proceeded under coordinating regeneration of TSCs, axon terminals, and receptor regions *(Kawabuchi et al., 2001)*. In the present study, examining the superposition of TSCs or axon terminals over receptor regions showed the precise reoccupation of former endplate sites by regenerated TSCs or axon terminals, within the territory of the receptor sites. The onset of endplate being reoccupied by regenerating SCs at 4 wpc coincides with the schedule that regenerating Schwann tubes and axons grow into the NMJ, and subsequent re-establishment of nerve-muscle contact is in process.

With increases of the superposition areas, a large proportion of the synapses' own terminal sprouts and endplates continue to be innervated by two or more distinct axons. In response to injury, NMJs enlarged due to multiple innervation and/or elaboration of the terminal arborization. Individual terminals sharing the polyaxonally innervated NMJs displayed some differences in superposition patterns, indicating discrepancy in the maturation process. The formation of multiple superpositions per NMJ may further confirm that the

size and complexity of axon terminals on individual endplates coincide with response for adaptation, remodeling, and maintenance of endplate structures documented for adult NMJs *(Barker and Ip, 1966; Cardasis and Padykula, 1981; Wernig and Herrera, 1986; Robbins and Polack, 1988)*. The major finding in this study is some characteristic profiles during endplate reoccupation and the difference in the regeneration pattern between TSCs and axon terminals, utilizing morphometric procedures of confocal 3D images for quantification of endplate reoccupation.

Characteristic morphological features during endplate reoccupation

On the endplate reoccupation, most of NMJs showed almost complete endplate realignment gradually after 4 wpc. We found some anomalous morphological features, especially in superposition between TSCs (or axon terminals) and AChR sites in NMJs, for example, occasional endplate vacancy (the area of the AChR site that has not reoccupied by regenerating axon terminals) with poorly developed synaptic contacts. Following nerve-crush injury, there was a moderate shrinkage of the AChR sites, which is consistent with the result reported by Csillik et al. *(1999)*. The subsequent events in this region denote coincidence of shrinkage and redifferentiation (reconstruction or new formation) within the same plaque *(Womble, 1986; Grady et al., 2000; Kawabuchi et al., 2001)*. The endplate realignment evidently commenced on the preexisting AChR plaques. After arriving at the endplate region, regenerating axon terminals appear to display some coordination in size and shape in superposition with the postsynaptic receptor regions *(Rich and Lichtman, 1989)*. Occasional endplate vacancy during the period of synapse realignment then suggests that a few conformational disorders, according to altered endplate geometry, may occur accidentally or transiently. Either the disproportionate growth rates between the pre- and postsynaptic regions or the poor growth of individual occupants are responsible for this disorder. In some NMJs, the AChR plaques may enlarge at a faster rate both laterally and longitudinally than the TSCs or axon terminals.

Early recovery of TSCs compared to axon terminals

In our previous study, we introduced the measure of overlap as calculated from the region of CC utilizing a dual-color confocal imaging technique *(Kawabuchi et al., 2001)*, the digitally subtracting procedure in the binary image for analysis of superimposed areas, as demonstrated in this communication. It is simple and repeatable and also useful to provide a reliable estimate of the extent of CC at the NMJ. As shown by the statistical data, the early recovery of the TSC-apposing contact areas compared to that of the axon terminals verifies differences in the regeneration patterns between these two endplate elements. It is potential that regeneration of the TSCs proceeds more rapidly at NMJs in order to reoccupy the postsynaptic receptor region sufficiently. In contrast, during the period of extensive growth of terminal branches in the synapse, the existing branches and bifurcation of motor nerve terminals elongated in a way that exactly matched the growth of receptor areas.

Normally, TSCs do not send processes into the synaptic gutter, and regeneration of the TSCs without invagination into the synaptic gutters may in part contribute to the early recovery of superposition areas in TSCs compared to axon terminals. Because TSCs engulf degenerating terminals and axons, and directly induce nerve terminal sprouts, they are likely to play important roles in facilitating successful reinnervation and regeneration in NMJs after nerve damage *(Son and Thompson, 1995a; 1995b; O'Malley et al., 1999; Kawabuchi et al., 2001)*. Certainly, adaptation to the synaptic environment during remodeling or regeneration is essential for TSCs to effectively modulate synaptic efficacy and neuronal activity *(Jahromi et al., 1992; Rochon et al., 2001)*. The rapid recovery in structures and superposition areas of TSCs after denervation suggests that they may be potential enough to exert a functional influence early in endplate reoccupation. Together with previous observations made using immunostaining *(Son and Thompson, 1995a; 1995b)*, the observations described here suggest that TSCs could be the substrate for nerve terminal and axon regeneration after nerve damage.

Anatomical relationship between presynaptic and postsynaptic elements

In development, the postsynaptic receptor region is an important determinant of endplate and terminal growth because postsynaptic regions grow at a faster rate than nerve terminals, and thus expansion of motor nerve terminals in NMJs is followed by postsynaptic growth *(Slack et al., 1983; Habgood and Hopkins, 1987)*. In regeneration, it has been suggested that receptors may be advantageous in the process of endplate reformation and may be in part important in the maintenance of regenerating nerve terminals, and that, in synaptic misalignment or their absence, nerve terminals are not maintained *(Rich and Lichtman, 1989; Balice-Gordon and Lichtman, 1990)*. In this study, a close correlation in the rates of size increase between the AChR sites and presynaptic elements suggests that the two elements are making alignment synchronously and reciprocally, and that the period when AChR sites progressively regenerate from shrinkage coincides with the period of growth of presynaptic elements. On the basis of this highly correlated

regeneration, we considered that the AChR site might be particularly important in promoting endplate regeneration. First, from early in reinnervation, pre-existing AChR sites provided the site where regeneration of TSCs and axon terminals proceeded. Secondly, it has been suggested that size increases in the developing postsynaptic site may initiate the growth of the axon terminal by some kind of contact-mediated interaction *(Nudell and Grinnel, 1983; Hopkins et al., 1985)*. In this study, the areas of CC and ratios of CC in TSCs or axon terminals represented the magnitudes of the spatial availability in relation to the AChR sites in regenerating NMJs. Indeed, we observed an ongoing recovery in this parameter of axon terminal- or TSC-mediated superposition. Finally, in our recent study, persistent damage of AChR sites was intimately associated with aging-related deterioration in reinnervation and regeneration of the endplates *(Kawabuchi et al., 2001)*. This evidence supports the possibility discussed above that the postsynaptic AChR sites contributed to the synaptic regeneration observed in NMJs. However, nerve injury primarily induces muscle atrophy, which accounts for not only decline of the trophic support for neurons but a reduction of neuronal support *(Johnson et al., 1995)*. Hence, it is important to note that a lot of evidence in recent years suggested that multiple cellular interactions between the pre- and postsyanptic elements, involving some local controls (via agrin, neuregulin, etc.), are necessary for synaptic reformation of the regenerating SCs, axons, and AChR sites in NMJs *(Kleiman and Reichardt, 1996; Denzer et al., 1997; Burden, 1998)*. This study does not address the possibility that the observed changes may provide direct and distinct proof for the synaptic interactions. However, on the basis of the frequent occurrence of unbalanced growth, for example, well-regenerated presynaptic regions contacting the malformed AChR sites (Figs. 4 and 5), the postsynaptic receptor region is unlikely to be an exclusive determinant for promoting endplate regeneration. It is concluded that a complex set of anatomical relationships between two or among the three endplate components affect the result of endplate reoccupation.

Persistent endplate reoccupation

We note that values of CC offer a tool to follow up the magnitude of morphological as well as potential physiological recovery in the pathway of reestablishment of synapse formation in regenerating NMJs. From ongoing recovery under lower CC values, we found persistent existence of incompletely occupied endplates, even up to 20 wpc. Anomalous synaptic disorder, such as greatly unoccupied AChR plaques and poorly formed individual occupants, was a consistent feature of these NMJs. This is compatible with the results from long-term observations on the pattern of reinnervation in which regenerated axons chronically exhibited pronounced morphological and physiological abnormalities for years *(Bowe et al., 1989)*. Following injury of peripheral nerves, the reasons for unsuccessful repair might come from two points, failure of axonal regeneration and the innervation of incorrect targets. The former derives from axon–SC interactions and other factors from peripheral glial cells, which are particularly important in nerve regeneration *(Ide et al., 1983; Scherer and Salzer, 1996)*. As for the latter, regenerating axons can cross endoneurial walls, even though the longitudinal continuity of these sheaths has been broken in crush lesions *(Brown and Hardman, 1987)*. Some mismatching is then possible when each proximal stump axon destines for its target via the endoneurial tube *(Fawcett and Keynes, 1990; Reynolds and Woolf, 1993)*. The establishment of precise spatial realignment could be a prerequisite to successful endplate regeneration. However, imperfect reinnervation and regeneration at the NMJ may give rise to sporadic remodeling during endplate reoccupation. Further investigation for the factors contributing to the mechanism of the spontaneous misalignment might be crucial in understanding the process in successful endplate regeneration.

Acknowledgements

We thank Mr. Takaaki Kanemaru (Morphology Core, Faculty of Medicine, Kyushu University) and Yasuhiro Hirakawa for their help in preparing photomicrographs. Grant Sponsor: Ministry of Education, Culture and Science of Japan; grant number: 12000210, 12670018 to M. K.

References

Balice-Gordon RJ, Lichtman JW (1990). In vivo visualization of the growth of pre- and postsynaptic elements of neuromuscular junctions in the mouse. J Neurosci 10:894–908.

Balice-Gordon RJ, Lichtman JW (1993). In vivo observations of pre- and postsynaptic changes during the transition from multiple to single innervation at developing neuromuscular junctions. J Neurosci 13:834–855.

Barker D, Ip MC (1966). Sprouting and degeneration of mammalian motor axons in normal and de-afferentated skeletal muscle. Proc R Soc Lond B Biol Sci 163:538–554.

Bowe CM, Hildebrand C, Kocsis JD, Waxman SG (1989). Morphological and physiological properties of neurons after long-term axonal regeneration: observations on chronic and delayed sequelae of peripheral nerve injury. J Neurol Sci 91:259–292.

Brown MC, Hardman VJ (1987). A reassessment of the accuracy of reinnervation by motoneurons following crushing or

freezing of the sciatic or lumbar spinal nerves of rats. Brain 110:695–705.
Burden SJ (1998). The formation of neuromuscular synapses. Genes Dev 12:133–148.
Cardasis CA, Padykula HA (1981). Ultrastructural evidence indicating reorganization at the neuromuscular junction in the normal rat soleus muscle. Anat Rec 200:41–59.
Crews LL, Wigston DJ (1990). The dependence of motoneurons on their target muscle during postnatal development of the mouse. J Neurosci 10:1643–1653.
Csillik B, Nemcsók J, Chase B, Csillik AE, Knyihár-Csillik E (1999). Infraterminal spreading and extrajunctional expression of nicotinic acetylcholine receptors in denervated skeletal muscle. Exp Brain Res 125:426–434.
Denzer AJ, Hauser DM, Gesemann M, Ruegg MA (1997). Synaptic differentiation: the role of agrin in the formation and maintenance of the neuromuscular junction. Cell Tissue Res 290:357–365.
Fawcett JW, Keynes RJ (1990). Peripheral nerve regeneration. Annu Rev Neurosci 13:43–60.
Glicksman MA, Sanes JR (1983). Differentiation of motor nerve terminals formed in the absence of muscle fibres. J Neurocytol 12:661–671.
Grady R, Zhou MH, Cunningham JM, Henry MD, Campbell KP, Sanes JR (2000). Maturation and maintenance of the neuromuscular synapse: genetic evidence for roles of the dystrophin–glycoprotein complex. Neuron 25:279–293.
Grinnell AD, Herrera AA (1981). Specificity and plasticity of neuromuscular connections: long term regulation of motoneuron function. Prog Neurobiol 17:203–282.
Habgood MD, Hopkins WG (1987). End-plate growth exceeds nerve terminal growth in juvenile mice. Exp Neurol 96:474–478.
Hall ZW, Sanes JR (1993). Synaptic structure and development: the neuromuscular junction. Cell 72:99–121.
Hirata K, Zhou C, Nakamura K, Kawabuchi M (1997). Postnatal development of Schwann cells at neuromuscular junctions, with special reference to synapse elimination. J Neurocytol 26:799–809.
Hopkins WG, Brown MC, Keynes RJ (1985). Postnatal growth of motor nerve terminals in muscles of the mouse. J Neurocytol 14:525–540.
Ide C, Tohyama K, Yokota R, Nitatori T, Onodera S (1983). Schwann cell basal lamina and nerve regeneration. Brain Res 288:61–75.
Jahromi BS, Robitale R, Charlton MP (1992). Transmitter release increases intracellular calcium in presynaptic Schwann cells in situ. Neuron 8:1069–1077.
Johnson H, Mossberg K, Arvidsson U, Piehl F, Hokfelt T, Ulfhake B (1995). Increase in alpha-CGRP and GAP-43 in aged motoneurons: a study of peptides, growth factors, and ChAT mRNA in the lumbar spinal cord of senescent rats with symptoms of hindlimb incapacities. J Comp Neurol 359:69–89.
Kawabuchi M, Zhou C, Islam ATM, Hirata K, Nada O (1998). The effect of aging on the morphological nerve changes during muscle reinnervation after nerve crush. Restor Neurol Neurosci 12:1–6.
Kawabuchi M, Zhou C, Wang S, Nakamura K, Liu WT, Hirata K (2001). The spatiotemporal relationship among Schwann cells, axons and postsynaptic acetylcholine receptor regions during muscle reinnervation in aged rats. Anat Rec 264:183–202.
Kleiman RJ, Reichardt LF (1996). Testing the agrin hypothesis. Cell 85:461–464.
Kuno M (1990). Target dependence of motoneuronal survival: the current status. Neurosci Res 9:155–172.
Navarro X, Verdu E, Wendelschafer-Crabb G, Kennedy WR (1997). Immunohistochemical study of skin reinnervation by regenerative axons. J Comp Neurol 380:164–174.
Nudell BM, Grinnell AD (1983). Regulation of synaptic position, size and strength in anuran skeletal muscle. J Neurosci 3:161–176.
O'Malley JP, Waran MT, Balice-Gordon RJ (1999). In vivo observations of terminal Schwann cells at normal, denervated, and reinnervated mouse neuromuscular junctions. J Neurobiol 38:270–286.
Reynolds ML, Woolf CJ (1993). Reciprocal Schwann cell-axon interactions. Curr Biol 3:683–693.
Rich MM, Lichtman JW (1989). In vivo visualization of pre- and postsynaptic changes during synapse elimination in reinnervated mouse muscle. J Neurosci 9:1781–1805.
Robbins N, Polak J (1988). Filopodia, lamellipodia and retractions at mouse neuromuscular junctions. J Neurocytol 17:545–561.
Rochon D, Rousse I, Robitaille R (2001). Synapse–glia interactions at the mammalian neuromuscular junction. J Neurosci 21:3819–3829.
Sanes JR (2003). The basement membrane/basal lamina of skeletal muscle. J Biol Chem 278: 12601–12604.
Sanes JR, Marshall LM, McMahan UJ (1978). Reinnervation of muscle fiber basal lamina after removal of myofibers. Differentiation of regenerating axons at original synaptic sites. J Cell Biol 78:176–198.
Scherer SS, Salzer JL (1996). Axon–Schwann cell interactions during peripheral nerve degeneration and regeneration. In: Glial Cell Development. Jessen KR, Richardson WD (Eds). Oxford Univeristy Press, London, Oxford, pp 165–196.
Slack JR, Pocket S, Macclement BAE (1983). Regulation of postnatal growth of motor endplates in rat soleus muscle. Exp Neurol 80:321–328.
Son YJ, Thompson WJ (1995a). Schwann cell processes guide regeneration of peripheral axons. Neuron 14:125–132.
Son YJ, Thompson WJ (1995b). Nerve sprouting in muscle is induced and guided by processes extended by Schwann cells. Neuron 14:133–141.
Trachtenberg JT, Thompson WJ (1997). Nerve terminal withdrawal from rat neuromuscular junctions induced by neuregulin and Schwann cells. J Neurosci 17:6243–6255.
Verdú E, Navarro X (1997). Comparison of immunohistochemical and functional reinnervation of skin and muscle after peripheral nerve injury. Exp Neurol 146:187–198.
Wernig A, Herrera AA (1986). Sprouting and remodeling at the nerve-muscle junction. Prog Neurobiol 27:251–291.
Womble MD (1986). The clustering of acetylcholine receptors and formation of neuromuscular junctions in regenerating mammalian muscle grafts. Am J Anat 176:191–205.

ELSEVIER

Journal of the Neurological Sciences 228 (2005) 87–92

Journal of the Neurological Sciences

www.elsevier.com/locate/jns

Th2 shift in juvenile muscular atrophy of distal upper extremity: a combined allergological and flow cytometric analysis

Manabu Osoegawa, Hirofumi Ochi, Feng-Jun Mei, Motozumi Minohara, Hiroyuki Murai, Takayuki Taniwaki, Jun-ichi Kira*

Department of Neurology, Neurological Institute, Graduate School of Medical Sciences, Kyushu University, Fukuoka 812-8582, Japan

Received 26 March 2004; received in revised form 1 October 2004; accepted 14 October 2004
Available online 24 November 2004

Abstract

Juvenile muscular atrophy of the distal upper extremity (JMADUE) is considered to be a type of flexion myelopathy; however, we recently reported cases of JMADUE associated with airway allergy successfully treated by plasma exchange. To further characterize the allergo-immunological features of JMADUE, 11 consecutive JMADUE patients in the neurology clinic at Kyushu University Hospital were studied. Past and present together with family histories of common allergic disorders were investigated. Total serum IgE was measured by an enzyme linked immunosorbent assay (ELISA) and allergen-specific IgE by a liquid phase enzyme immunoassay. Intracellular interferon (IFN) γ-, interleukin (IL)-4-, IL-5- and IL-13-producing T cells in peripheral blood were analyzed by flow cytometry. Data from 42 healthy subjects were used as controls for allergological studies. Flow cytometric data from 21 healthy subjects were also used for comparison. The patients exhibited significantly higher frequencies of coexisting airway allergies such as allergic rhinitis (p=0.0057) and pollinosis (p=0.0064), family histories of allergic disorders (p=0.0075), and mite antigen specific IgE (p=0.0361) compared with the healthy subjects. Patients with JMADUE had a significantly higher percentage of IFNγ$^-$IL-4$^+$CD4$^+$T cells (p=0.0017), but not IL-5- or IL-13-producing CD4$^+$T cells, and a reduced intracellular IFNγ/IL-4 ratio in CD4$^+$T cells (p=0.002) compared to the controls. These findings suggest that JMADUE has a significant T helper 2 (Th2) shift, which may in part contribute to the development of spinal cord damage.

Keywords: Flow cytometry; Hirayama disease; Atopy; IgE

1. Introduction

Juvenile muscular atrophy of the distal upper extremity (JMADUE), or Hirayama disease, is a rare disease that affects adolescents and is characterized by unilateral or asymmetric muscular atrophy and weakness in the hand and forearm [1,2]. The disease initially develops progressively, but is followed by spontaneous arrest several years after onset. The precise mechanism of this condition remains unclear, although contributing factors include a mechanical force pressing on the lower cervical cord and some microcirculatory deficiencies [1,3]. We have recently shown that this condition is closely associated with airway allergies, such as allergic rhinitis and bronchial asthma [4], and reported two cases associated with an airway allergy that were successfully treated by plasma exchange [5]. These reports indicate that atopy and its related immune aberration may contribute to the development of this condition.

In immune mediated diseases, the T helper 1 (Th1) and T helper 2 (Th2) cytokine balance plays a critical role [6]. The cytokine balance in JMADUE has not been reported. Therefore, in the present study, we aimed to determine the Th1/Th2 balance by flow cytometrically measuring the percentage of intracellular interferon (IFN)γ-, interleukin (IL)-4-, IL-5- and IL-13-producing T cells in peripheral blood CD4$^+$T cells and CD8$^+$T cells, and to clarify coexistent allergic conditions in 11 consecutive patients with JMADUE.

* Corresponding author. Tel.: +81 92 642 5340; fax: +81 92 642 5352.
E-mail address: kira@neuro.med.kyushu-u.ac.jp (J. Kira).

0022-510X/$ - see front matter © 2004 Elsevier B.V. All rights reserved.
doi:10.1016/j.jns.2004.10.003

2. Subjects and methods

2.1. Subjects

Eleven consecutive patients exhibiting JMADUE (two women and nine men, mean age 18 (range 13–22) years at the time of examination in the neurology clinic at Kyushu University Hospital) were enrolled in this study. Patients one through five were the same as those in a previous report [4].

2.2. Methods

Cervical MRI was performed in a neutral, and fully flexed position to examine the forward displacement of the dural sac and flattening of the lower cervical cord. All patients were questioned about their history of allergic disorders, such as bronchial asthma, allergic rhinitis, pollinosis, atopic dermatitis, allergic conjunctivitis, urticaria, and allergies to food, metals and drugs. Total serum IgE levels were measured by an enzyme linked immunosorbent assay (ELISA) and specific IgE to antigens such as *Dermatophagoides* (*D.*) *farinae*, *D. pteronyssinus*, cedar pollen, Candida, egg white, milk, wheat, rice, and soya bean were measured by a liquid phase enzyme immunoassay (Ala-STAT, Sankoujunyaku, Tokyo, Japan). A serum IgE concentration higher than 250 U/ml was considered to be hyperIgEaemia, and a cut off value for allergen specific IgE was set at 0.34 IU/ml in accordance with the manufacturer's instruction. The frequency of coexisting allergic disorders, hyperIgEaemia and allergen specific IgE, was determined by comparison with neurologically normal control data of 42 co-workers in the neurology clinic at Kyushu University Hospital, after obtaining their informed consent (mean age±S.D.=34.0±8.3 years, 22 male and 20 females).

Intracellular IFNγ, IL-4, IL-5 and IL-13 production from peripheral blood $CD4^+$ and $CD8^+$T cells were analyzed as described previously [7,8]. Briefly, peripheral blood-derived mononuclear cells were treated for 4 h with 25 ng/ml phorbol 12-myristate 13-acetate (Sigma, St. Louis, MO, USA) and 1 μg/ml of ionomycin (Sigma) in the presence of 10 μg/ml brefeldin A (Sigma). After washes with phosphate-buffered saline containing 0.1% bovine serum albumin (0.1% BSA-PBS), the cells were stained with PerCP-conjugated anti-CD4 (13B8.2, Becton Dickinson, San Jose, CA, USA) or anti-CD8 (1B9.2, Becton Dickinson) monoclonal antibody in the dark for 15 min at room temperature. Cells were washed twice, permeabilized with FACS permeabilizing solution (Becton Dickinson) and incubated with FITC-conjugated anti-IFNγ (clone 25723.11, Becton Dickinson) and PE-conjugated anti-IL-4 (clone 3010.211, Becton Dickinson), or either anti-IL-5 (JES1-39D10, PharMingen, San Diego, CA) or anti-IL-13 (JES10-5A2, PharMingen) monoclonal antibody in the dark at room temperature for 30 min. Corresponding isotype-matched antibodies were used as negative controls. As the last step, cells were washed with 0.1% BSA-PBS and resuspended in 1% paraformaldehyde for subsequent two-color flow cytometric analysis using an Epics XL System II (Coulter, Hialeah, FL, USA). Ten thousand events per lymphocyte were acquired and analyzed. Analysis gates were set on lymphocytes according to the forward and side scatter properties and then further gated on $CD4^+$ and $CD8^+$ cells, respectively. $CD8^+$ cells were divided into $CD8^{high}$ and $CD8^{low}$ [7]. Many $CD8^{low}$ cells expressed both CD16 and CD56 and, therefore, were considered to be natural killer cells. In contrast, virtually all $CD8^{high}$ cells expressed CD3 but not CD16 (data not shown). We therefore defined $CD8^{high}$ cells as $CD8^+$T cells. Flow cytometric data from patients with JMADUE was compared with data of 21 neurologically normal control subjects (30.5±6.2 years, 13 males and 9 females).

Statistical analysis for cell percentage comparison was performed using the Bonferroni/Dunn test with one-way factorial ANOVA. Either the chi-square test or Fisher's exact test (when the criteria of the chi-square test was not fulfilled) was used for the analysis of the frequency of atopic disorders, hyperIgEaemia and allergen-specific IgE.

3. Results

3.1. Clinical findings

During the 6-year analysis period, 11 consecutive patients (2 women and 9 men) exhibiting JMADUE were seen at our Institute (Table 1). The age of onset ranged from 12 to 18 years old (15.8±1.9), and the duration of the disease was 3 months to 7 years (2.5±1.9 years) at the time of examination. All showed gradual onset of unilateral or asymmetrical muscular atrophy and weakness in the distal parts of their upper extremities. Needle electromyogram revealed either on-going or chronic denervation potentials in the affected muscles of all patients. Cerebrospinal fluid examinations were all normal in the six patients who underwent lumbar puncture in our clinic. Cervical MRIs in a neutral position were normal, except for patient 6 who exhibited a high intense lesion in the left anterior horn on T2-weighted images at the C5-6 spine level not enhanced by gadolinium-DTPA. Cervical MRI in a fully flexed position of the neck showed 10 patients with a flattening of the lower cervical cord, but of these only six exhibited forward displacement of the dural sac together with an intense crescent-shaped signal behind the cord. One patient (patient 11) showed neither cord flattening nor a crescent-shaped signal. Two patients (patients 6 and 9) responded to plasma exchange and have been reported elsewhere [5].